

## Self-pierce riveting of multiple steel and aluminium alloy sheets

K. Mori<sup>a,\*</sup>, Y. Abe<sup>a</sup>, T. Kato<sup>b</sup>

<sup>a</sup> Department of Mechanical Engineering, Toyohashi University of Technology, Tempaku, Toyohashi, Aichi, 441-8580, Japan

<sup>b</sup> Department of Mechanical Engineering, Ishikawa College of Technology, Kahoku-gun, Ishikawa 929-0392, Japan.

\* Corresponding author. Tel.: +81 532 44 6705; Fax.: 81 532 44 6690.

E-mail address: mori@plast.me.tut.ac.jp (K. Mori)

### ABSTRACT

Multiple steel and aluminium alloy sheets were joined by self-pierce riveting. Self-pierce riveting is attractive for joining multiple and dissimilar sheets, because joining of individual interfaces is not necessary unlike the conventional joining processes, i.e. sheets except for a lower sheet are merely pieced with a rivet shirt. The steel sheets ranged from mild steel to ultra-high strength one having 980 MPa in tensile strength, and the joinability for three steel and aluminium alloy sheets for various combinations was examined from both experiments and finite element simulation. The joinability was improved by setting a softer sheet uppermost due to smooth piercing. In addition, the joining range for self-pierce riveting of three high strength steel and aluminium alloy sheets was extended by optimising a shape of the die, and the ultra-high strength steel, mild steel and aluminium alloy sheets were successfully joined.

*Keywords:* joining, self-pierce riveting, multiple sheets, high strength steel sheet, aluminium alloy sheet.

### 1. Introduction

The reduction in weight of automobiles is significantly effective in improving fuel consumption, and thus high strength steel and aluminium alloy sheets with high specific strengths are increasingly used in automobile body panels (Lai and Brun, 2007). It is not easy to form high strength steel and aluminium alloy sheets because of large springback and small formability. Mori et al. (2007) reduced the springback in bending of ultra-high strength steel sheets by bottoming having small reduction in thickness at the bottom dead centre by means of a servo press. Mori et al. (2010) improved the hole expansion of a punched ultra-high strength steel sheet by smoothing fracture surface of the sheared edge using a conical punch. Sartkulvanich et al. (2010) predicted the occurrence of cracks in hole expansion of a punched high strength steel sheet from finite element simulation. Abe et al. (2013) developed a gradually contacting punch for increasing stretch flangeability of ultra-high strength steel sheets. Since high strength steel and aluminium alloy sheets are often used together, reliable joining processes for these dissimilar materials are required. As the melting temperatures of steel and aluminium are very different, conventional fusion welding and resistance welding are not suitable for joining sheets made of these materials.

The development of joining processes of multiple sheets leads to improvement of design flexibility of automobile body panels. For example, the use of reinforcements increases to heighten the cash safety and joining of multiple sheets is required because of the addition of

the reinforcements. In the present manufacturing of automobiles, resistance spot welding of three steel sheets comes up to one third of total welded joints, while it is not easy to find appropriate welding conditions for multiple sheets. Ma and Murakawa (2010) examined formation of a nugget in resistance spot welding of three high strength steel sheets from both finite element simulation and experiment. It is desirable to develop a joining process of multi aluminium alloy and steel sheets. Although adhesive bonding is available for joining multi sheets, the strength and degradation of the bonded joints are still unacceptable for the body panels. For mechanical joining with screws and rivets, pre-drilling operations are needed and stress concentration appears around edges of holes.

The use of plastic deformation for joining workpieces is very advantageous to dissimilar materials in order to avoid the difficulty of melting point. Mori et al. (2013) reviewed various joining processes by plastic deformation and demonstrated their effectiveness and applicability. Abe et al. (2012) joined high strength steel and aluminium alloy sheets by mechanical clinching, and Coelho et al. (2012) employed friction stir welding for joining of these sheets. Since plastic deformation in workpieces is distributed during mechanical clinching and friction stir welding, it is not easy to control plastic deformation for attaining proper joining of all interfaces for multiple sheets.

Self-pierce riveting is a cold process for joining sheets by driving a rivet through the upper sheet and by flaring a skirt of the rivet in the lower sheet to create an interlock. The sheets are joined by hooking the lower sheet on the flared skirt under embedding the rivet in the upper sheet. Barnes and Pashby (2000) reported the application of self-pierce riveting to automobile body panels. He et al. (2008) reviewed self-pierce riveting processes. Since this riveting process does not require a pre-drilled hole unlike the conventional riveting processes, the joining speed is the same level with that of spot welding, and the equipment is also similar. Mori et al. (2012) explored the mechanism of superiority of fatigue strength for self-pierce riveting. Neugebauer et al. (2011) demonstrated the improvement of joinability for high speed self-pierce riveting.

Although self-pierce riveting is mainly employed for joining of aluminium alloy sheets, self-pierce riveting can be applied to dissimilar sheet metals because of cold joining. Abe et al. (2006) categorised defects for the self-pierce riveting of aluminium alloy and steel sheets to obtain optimum joining conditions. In addition, Mori et al. (2006) joined aluminium alloy and high strength steel sheets with self-pierce riveting, and Abe et al. (2009) optimised shapes of the dies for joining of aluminium alloy and high strength steel sheets. Not only two sheets but also more than three sheets can be joined by self-pierce riveting. Kato et al. (2007) reported self-pierce riveting of three aluminium alloy sheets.

In the present paper, the mechanism of self-pierce riveting of multiple aluminium alloy and steel sheets was examined. The deforming behaviour in the self-pierce riveting processes of steel and aluminium alloy sheets was examined from finite element simulation and experiments to evaluate optimum joining conditions.

## **2. Self-pierce riveting process of multiple sheets**

### *2.1. Joining mechanism of multiple dissimilar sheets*

Multiple aluminium alloy and steel sheets were joined by self-pierce riveting without heating to solve the problem of the different melting temperatures. In self-pierce riveting, the sheets are pierced with a tubular rivet without pre-drilling as shown in Fig. 1. The rivet is driven through the sheets except for the lower sheet and the skirt of the rivet is flared in the lower sheet. The multiple sheets are joined by the interlock between the lower sheet and the

flared skirt of the rivet, hooking the lower sheet on the flared skirt. Successful joining of sheets in self-pierce riveting requires:

- driving rivet skirt through sheets except for lower sheet,
- interlock formation by flaring rivet skirt in lower sheet,
- no fracturing of lower sheet.

When the rivet skirt is not driven through the sheets except for the lower sheet, the sheets do not join, i.e. the interlock in the lower sheet is not formed. The fracture of the lower sheet leads to corrosion. Enough ductility of the sheets is essential to joining, particularly for the lower sheet. The joinability of multiple sheets is influenced by the flow stress, ductility and combination of the sheets, the mechanical properties of the rivet, the die shape, etc. Although the sheets are not heated in self-pierce riveting, the differences of flow stress and ductility between multiple sheets are problematic, particularly very hard ultra-high strength steel and soft aluminium alloy sheets.

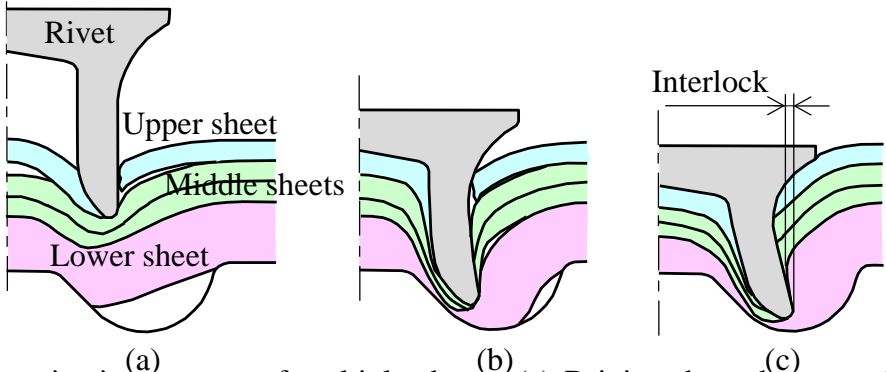


**Fig. 1.** Self-pierce riveting process of multiple sheets. (a) Driving through upper sheet, (b) driving through sheets except for upper sheets and (c) joining by formation of interlock.

Self-pierce riveting is attractive for joining multiple and dissimilar sheets, because joining of individual interfaces is not necessary unlike the conventional joining processes. The sheets except for the lower sheet are merely pierced with the rivet. Particularly in self-pierce riveting of multiple similar sheets shown in Fig. 2, the sheets except for the lower sheet behave like one upper sheet, and the joining operation of multiple sheets is similar to that of two sheets. This leads to easy design of the process.

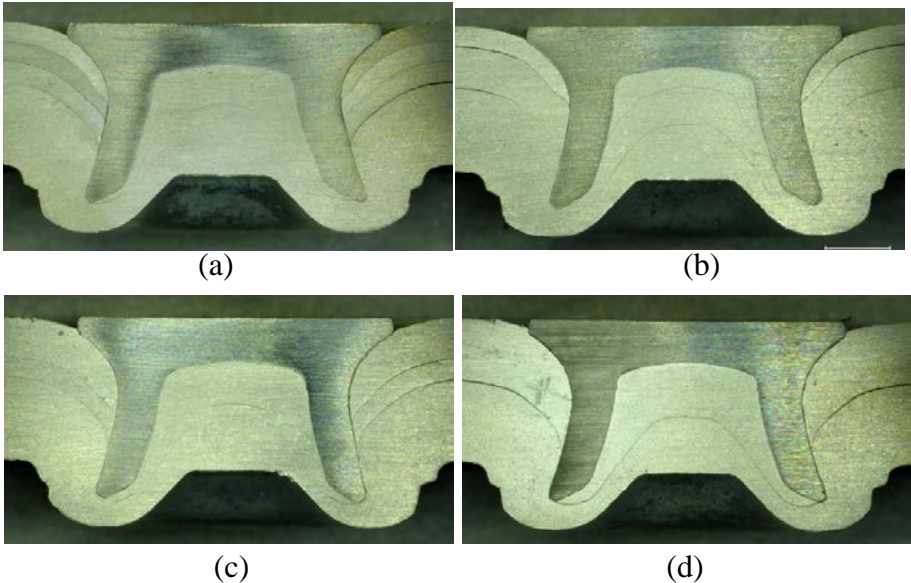


**Fig. 2.** Self-pierce riveting of multiple aluminium alloy A5052-H34 sheets having thicknesses of (a) 0.5-0.5-0.5-2 mm, (b) 0.5-1-2 mm, (c) 1-0.5-2 mm and (d) 1.5-2 mm.

## 2.2. Joining procedure

The tools used for the experiment of self-pierce riveting are illustrated in Fig. 3. The aluminium alloy sheet A5052-H34 typically used for automobile body panels was chosen, and the steel sheets have different nominal tensile strengths shown in Table 1. The rivet is made of boron steel and is plated with zinc to prevent corrosion after the riveting. The flow stresses of the sheets and rivet were measured from the uniaxial tensile and compression tests, respectively. The sheets were fixed with the sheet holder and die, and were joined by driving the rivet with the punch. The rivet and die are the same as the joining of two sheets.

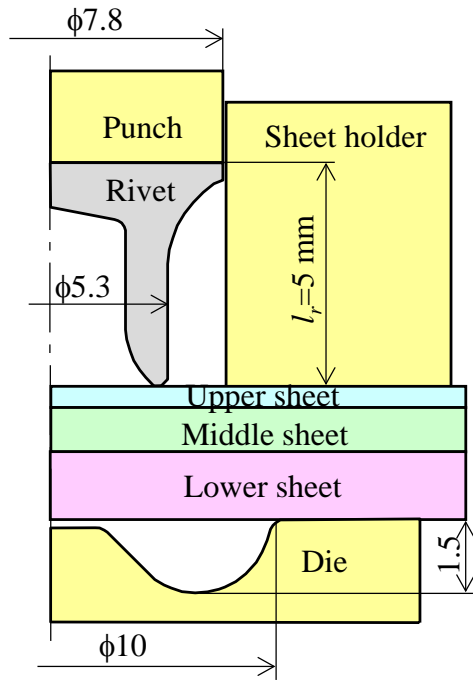


**Fig. 3.** Tools used for experiment of self-pierce riveting.

**Table 1**

Mechanical properties of sheets and rivet used for self-pierce riveting.

Sheet	Material	Thickness [mm]	Elongation [%]	Yield stress [MPa]	Tensile strength [MPa]	Flow stress curve [MPa]
SPCC (S1)	Mild steel	1.0	33	203	334	$\sigma = 530 \varepsilon^{0.25}$
SPFC440 (S2)	Dual-phase steel	1.0	25	343	473	$\sigma = 774 \varepsilon^{0.18}$
SPFC590 (S3)		1.0	18	424	623	$\sigma = 979 \varepsilon^{0.16}$
SPFC780 (S4)		1.0	20	503	764	$\sigma = 1187 \varepsilon^{0.15}$
SPFC980 (S5)		1.0	17	838	976	$\sigma = 1337 \varepsilon^{0.08}$
		2.0	18	862	1057	$\sigma = 1531 \varepsilon^{0.13}$
A5052-H34 (A1)	Aluminium-magnesium alloy	1.0	8.2	205	258	$\sigma = 387 \varepsilon^{0.12}$
		2.5	9.3	196	244	$\sigma = 353 \varepsilon^{0.11}$
Rivet	0.35%-carbon boron steel			1850		$\sigma = 1955 \varepsilon^{0.014}$

The self-pierce riveting process of the sheets was simulated by the commercial finite element code LS-DYNA. Axi-symmetric deformation was assumed by limiting the calculation to the vicinity undergoing plastic deformation. The cross-sections of the sheets and rivet were divided into quadrilateral solid ring elements. Not only the sheets but also the rivet undergoes plastic deformation during the riveting. The die, punch and sheet holder were assumed to be rigid. The coefficient of friction at the interface between the rivet and sheet equivalent to an unlubricated condition in the simulation was 0.20. The flow stress curves of the sheets and rivet used for the finite element simulation measured from the tensile and compression tests, respectively, are given Table 1.

### 3. Self-pierce riveting process of three mild steel and aluminium alloy sheets

#### 3.1. Deformation behaviour of sheets and rivet

The deforming behaviour of the rivet and sheets obtained from the finite element simulation of self-pierce riveting of the upper and lower aluminium alloy A5052-H34 and middle mild steel SPCC sheets for  $t_u=0.5$  mm,  $t_m=1.2$  mm and  $t_l=1.5$  mm is shown in Fig. 4, where  $s$  is the punch stroke. When the aspect ratios of elements deteriorated, elements were deleted, as fracture would occur. This leads to simple treatment without damage models. The rivet skirt is driven through the upper and middle sheets, and then the skirt is flared with the die without penetration in the lower sheet. The three sheets are successfully joined.

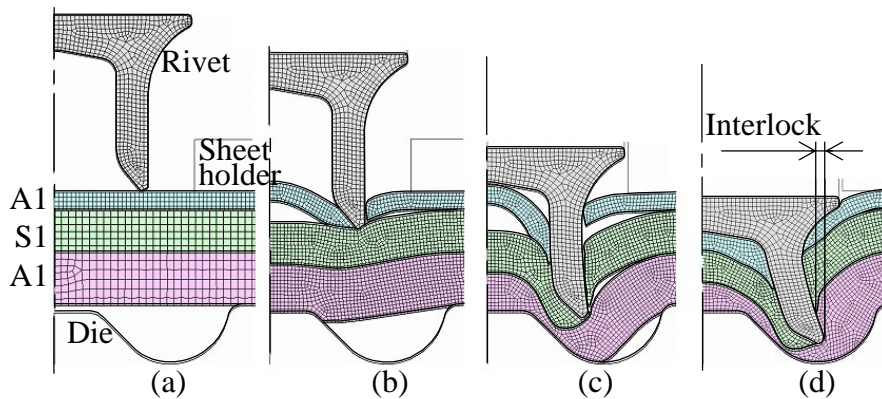


**Fig. 4.** Deforming behaviour of rivet and sheets obtained from finite element simulation of self-pierce riveting of upper and lower: A5052-H34 (A1) and middle: SPCC (S1) for  $t_u=0.5$  mm,  $t_m=1.2$  mm and  $t_l=1.5$  mm. (a)  $s=0.0$  mm, (b)  $s=1.0$  mm, (c)  $s=3.8$  mm and (d)  $s=5.0$  mm.

The cross-sectional shapes of the rivet and sheets obtained from the experiment under the same conditions with the calculation of Fig. 4 are illustrated in Fig. 5. The calculated result shown in Fig. 4 (d) is in good agreement with the experimental one.

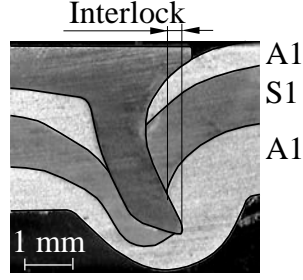


**Fig. 5.** Cross-sectional shapes of rivet and sheets obtained from experiment of riveting of upper and lower: A5052-H34 (A1) and middle: SPCC (S1) for  $t_u=0.5$  mm,  $t_m=1.2$  mm and  $t_l=1.5$  mm.

### 3.2. Joinability

The ratio,  $R_l$ , of the thickness of the lower sheet to the total thickness  $t_{all}$  and the ratio,  $R_{all}$ , of the total thickness to the length,  $l_r$ , of the rivet skirt shown in Fig. 3 are given by

$$R_l = t_l / t_{all} \quad (1)$$

$$R_{all} = t_{all} / l_r \quad (2)$$

The defects for the self-pierce riveting of the two aluminium alloy and one steel sheet are given in Fig. 6. In Fig. 6(a) for the upper mild sheet, the rivet skirt is not driven through the middle sheet, and thus the three sheets are not joined. In Fig. 6(b) for the upper aluminium alloy sheet, the lower sheet ruptures, and thus the risk of corrosion leading to the reduction in strength is caused.

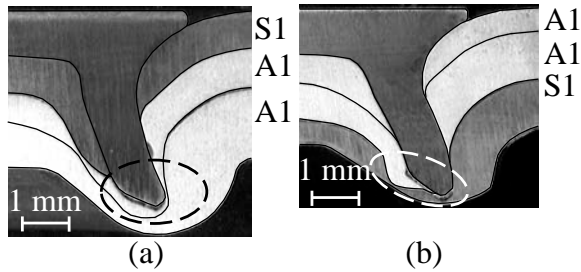


**Fig. 6.** Defects for self-pierce riveting. (a) No driving through middle sheet, upper: SPCC (S1), middle and lower: A5052-H34 (A1),  $t_u=t_m=0.8$  mm,  $t_l=1.5$  mm and (b) rupture of lower sheet, upper and middle: A5052-H34 (A1), lower: SPCC (S1),  $t_u=0.5$  mm,  $t_m=t_l=1.0$  mm.

The joinability for the three sheets obtained from the experiment is shown in Fig. 7. When the ratio,  $R_l$ , of the thickness of the lower sheet to the total thickness is small and the ratio,  $R_{all}$ , of the total thickness to the length of the rivet skirt is large, no driving through the middle sheet occurs. When the ratio,  $R_{all}$ , of the total thickness to the length of the rivet skirt is small, the lower sheet ruptures due to the excessive length of the rivet skirt. It is required that the length of the rivet skirt is adjusted to the thicknesses of the sheets. However, this leads to the increase in pattern of the rivet. The joinability exhibits a similar tendency for all combinations.

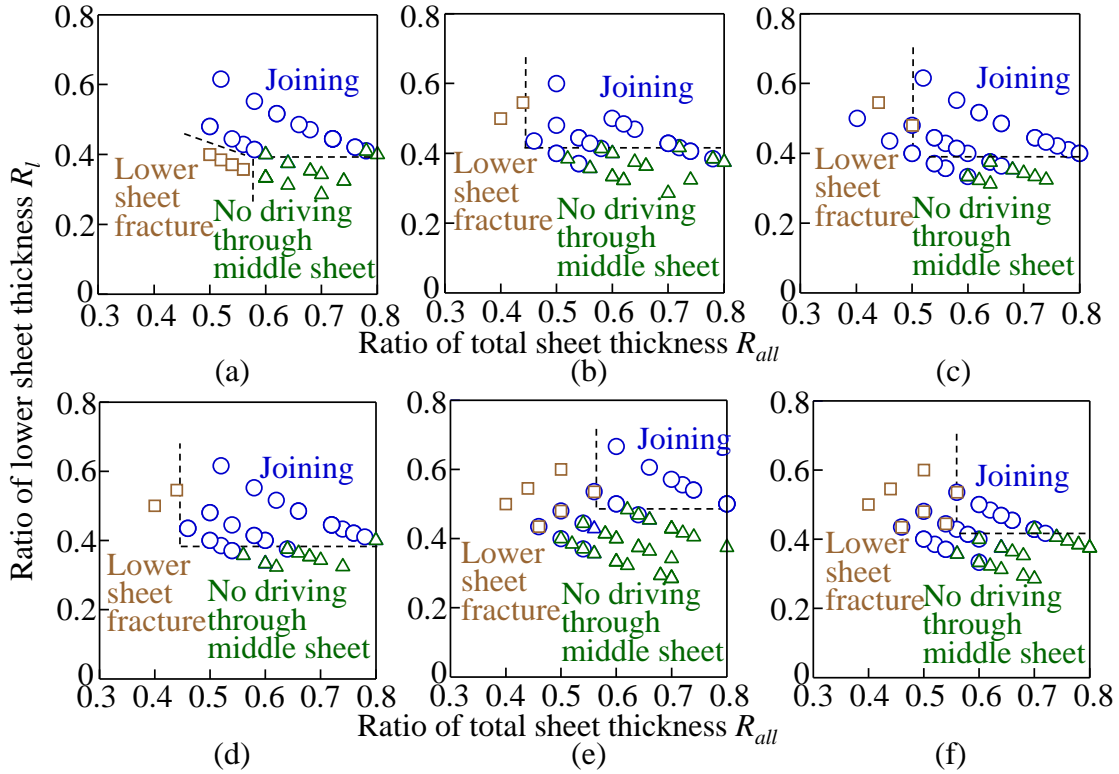


**Fig. 7.** Joinability for three sheets obtained from experiment. (a) Upper and middle: aluminium, lower: steel, (b) upper and middle: steel, lower: aluminium, (c) upper: aluminium, middle and lower: steel, (d) upper and lower: steel, middle: aluminium, (e) upper: steel, middle and lower: aluminium and (f) Upper and lower: aluminium, middle: steel.

### 3.3. Effect of combination of sheets except for lower sheet

In joining of similar sheets shown in Fig. 2, the joinability was independent of the combination of sheets except for the lower sheets, whereas the joinability is influenced by the combination for dissimilar sheets as shown in Fig. 8. In the upper aluminium and middle mild steel sheets, the interlock was formed, and the formation failed for the reverse combination.

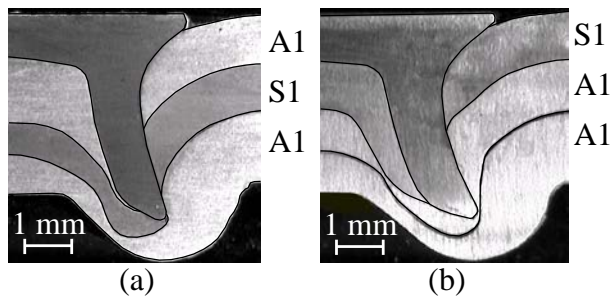


**Fig. 8.** Comparison between cross-sectional shapes obtained from experiment for  $t_u = t_m = 1.0$  mm,  $t_l = 1.5$  mm. (a) Upper and lower: A502-H34 (A1), middle: SPCC (S1) and (b) Upper: SPCC (S1), middle and lower: A502-H34 (A1).

The variations in calculated riveting load with the punch stroke for the two combinations of the upper and middle sheets are illustrated in Fig. 9. Although the joinability is influenced by the combination as shown in Fig. 8, the riveting loads are similar.



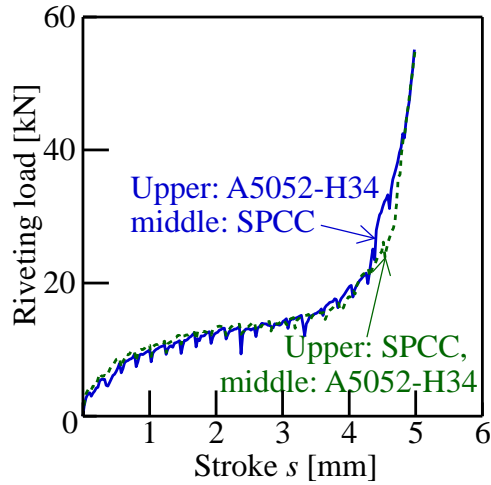


**Fig. 9.** Comparison between riveting loads from finite element simulation for  $t_u = t_m = 1.0$  mm,  $t_l = 1.5$  mm.

The calculated deformation behaviour of the sheets and rivet for the reverse combinations of the upper and middle sheets is illustrated in Fig. 10. Piercing of the rivet was delayed by the stronger upper steel, the cavity between the rivet and upper sheet remained in the intermediate stage, and thus the interlock was not formed.

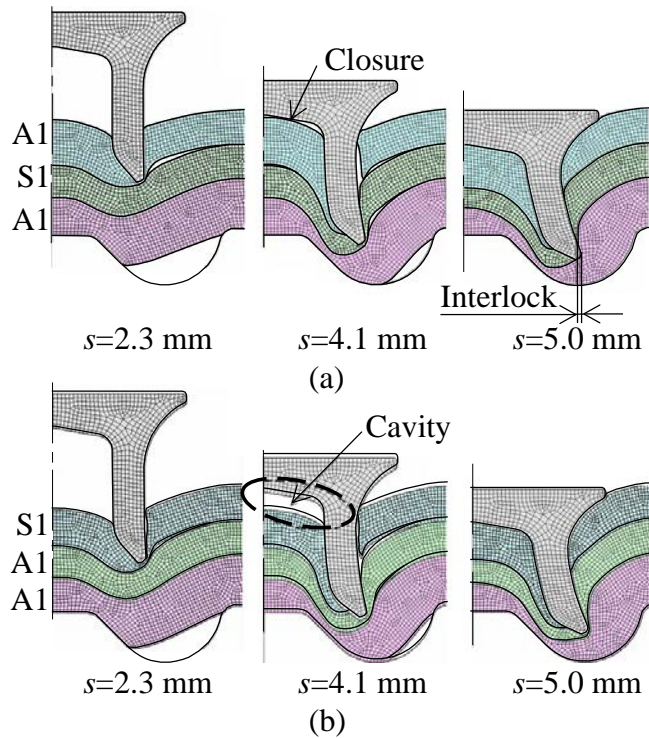


**Fig. 10.** Deforming behaviour of rivet and sheets obtained from finite element simulation for  $t_u = t_m = 1.0$  mm,  $t_l = 1.5$  mm. (a) Upper and lower: A5052-H34 (A1), middle: SPCC (S1) and (b) upper: SPCC (S1), middle and lower: A5052-H34 (A1).



### 3.4. Strength of joint

The strength of the joined sheets was measured from the cross-tension test shown in Fig. 11. The upper sheet is pulled under fixing the lower sheet, whereas the middle sheet is free.

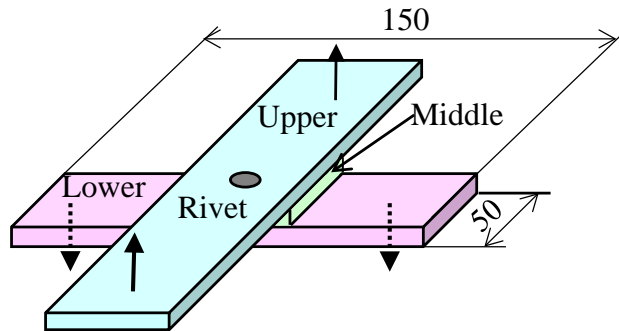


**Fig. 11.** Cross-tension test for measuring strength of joints.

The fractures in the cross-tension test for the upper and lower aluminium and the middle steel sheets are illustrated in Fig. 12. In Fig. (a), the head of the rivet slips from the fractured upper sheet, and this fracture is dependent on the strength of the upper sheet. In Fig. (b), the rivet skirt slips from the lower sheet, and this fracture is dependent on the amount of interlock.

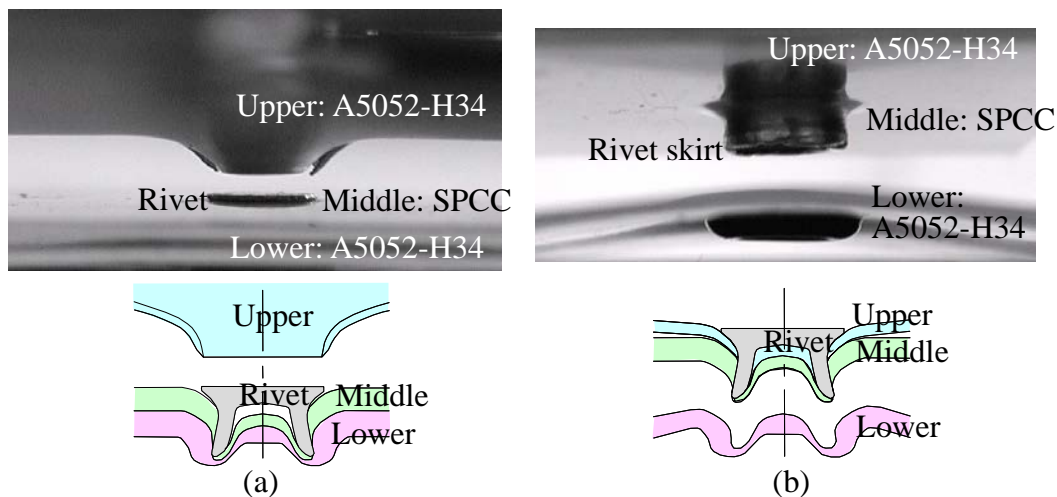


**Fig. 12.** Fractures in cross-tension test for upper and lower: A5052-H34 and middle: SPCC. (a) Fracture of upper sheet,  $t_u=0.5$  mm,  $t_m=1.2$  mm,  $t_l=1.5$  mm and (b) fracture of lower sheet,  $t_u=0.8$  mm,  $t_m=1.2$  mm,  $t_l=1.0$  mm.

The relationship between the maximum load and the interlock area in the cross-tension test for one steel and two aluminium alloy sheets is given in Fig. 13. As the interlock area increases, the maximum load increases. The amount of interlock has a significant effect on the maximum load, because the interlock functions as a hook of the lower sheet. On the other hand, the maximum load for the lower steel sheet is larger than that for the lower aluminium alloy sheet, because the hook of the steel sheet is stronger.

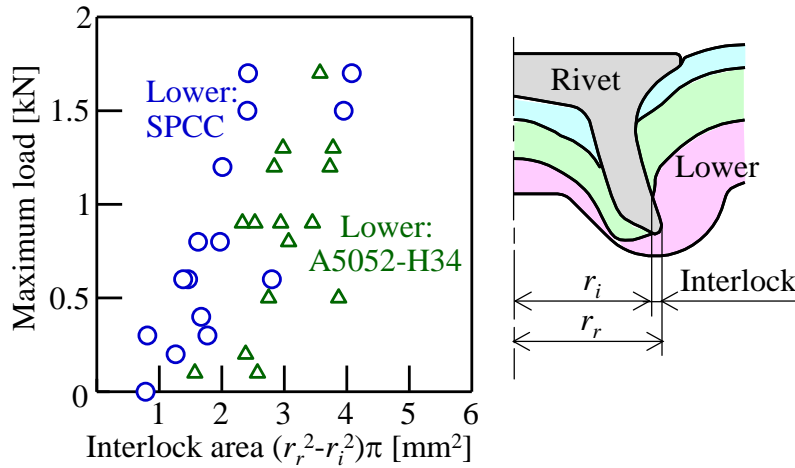


**Fig. 13.** Relationship between maximum load and interlock area in cross-tension test for one mild steel and two aluminium alloy sheets.

#### 4. Joining of three high strength steel and aluminium alloy sheets

##### 4.1. Joinability

Three high strength steel and aluminium alloy sheets were joined by self-pierce riveting. Since the strength of the high strength steel sheets is large, it is not easy to drive the rivet skirt through the sheets. The thickness of the sheet used for automobiles generally decreases with increase in strength because of the reduction in weight. In self-pierce riveting, it is inadequate to set a thin and hard sheet at the lower side due to fracture of the lower sheet, and thus the lower sheet was fixed to the aluminium alloy one having 2.5 mm in thickness in this chapter. The strengths of the upper and middle steel sheets having 1 mm in thickness were changed to examine the joinability.

The effect of the combination of the upper and middle sheets on the joinability is shown in Fig. 14. For the upper mild steel sheet, the interlock is formed, whereas the lower sheet is not pierced with the rivet skirt for upper SPFC980. The joinability is influenced by the combination of sheets.

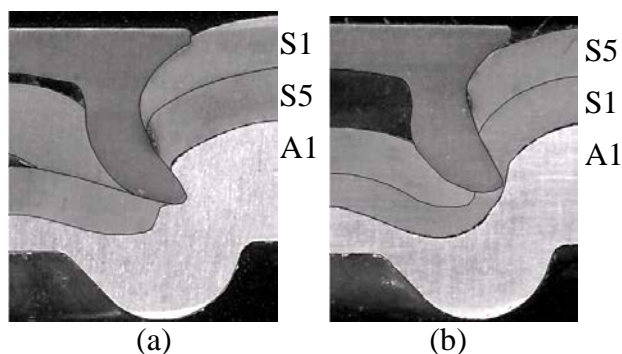


**Fig. 14.** Comparison between cross-sectional shapes for (a) upper: SPCC (S1), middle: SPFC980 (S5) and (b) upper: SPFC980 (S5), middle: SPCC (S1).

The calculated deformation behaviour of the sheets and rivet for the same combinations as Fig. 14 is illustrated in Fig. 15. For the upper mild steel sheet, piercing with the rivet skirt is smooth. On the other hand, the tip of the rivet skirt is largely compressed by upper SPFC980 and it is delayed to pierce the upper and middle sheets. Since the tip of the rivet skirt is shifted

from the centre to flare the skirt during piercing, the tip is dulled by the hard upper sheet, and thus driving through the lower sheet becomes insufficient.

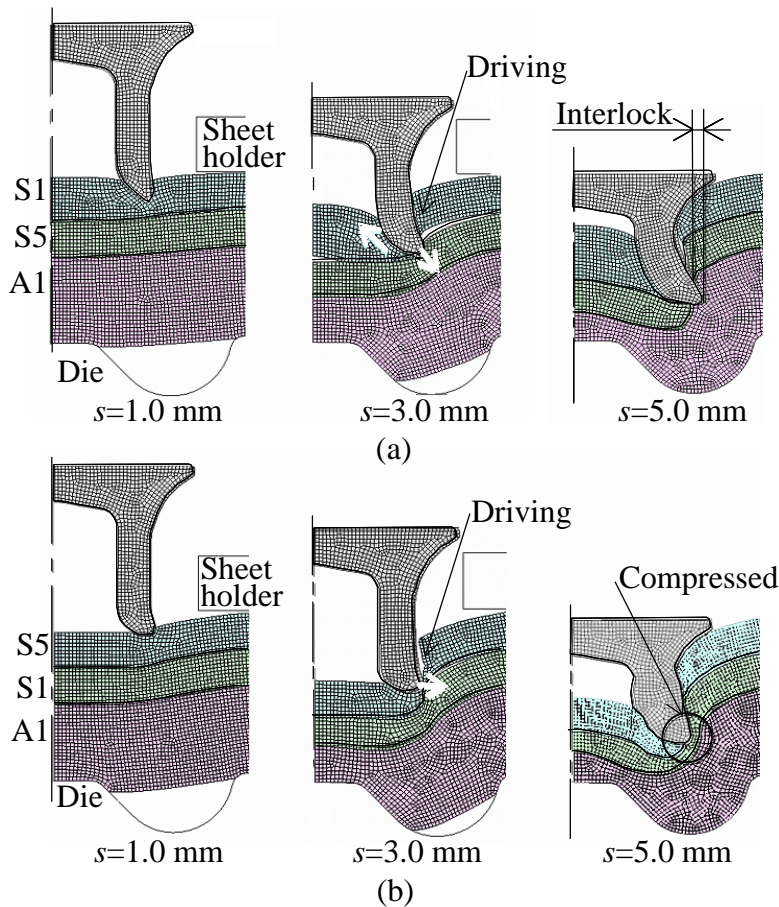


**Fig 15.** Deforming behaviour of rivet and sheets obtained from finite element simulation of self-pierce riveting of high strength steel, mild steel and aluminium alloy sheets for  $t_u = t_m = 1$  mm,  $t_l = 2.5$  mm. (a) Upper: SPCC (S1), middle: SPFC980 (S5) and (b) upper: SPFC980 (S5), middle: SPCC (S1).

The effects of the strengths of the upper and middle sheets on the joinability for the upper and middle steel sheets and the lower aluminium alloy sheets for  $t_u = t_m = 1.0$  mm,  $t_l = 2.5$  mm are given in Fig. 16. As the strengths of the upper and middle sheets increase, the joinability deteriorates. When the upper sheet is SPFC780 and SPFC980, the rivet was not driven through the middle sheet for all combinations. On the other hand, joining was attained for the upper sheets having smaller strength than SPFC440. It was found that the joinability is improved by setting a softer sheet uppermost.

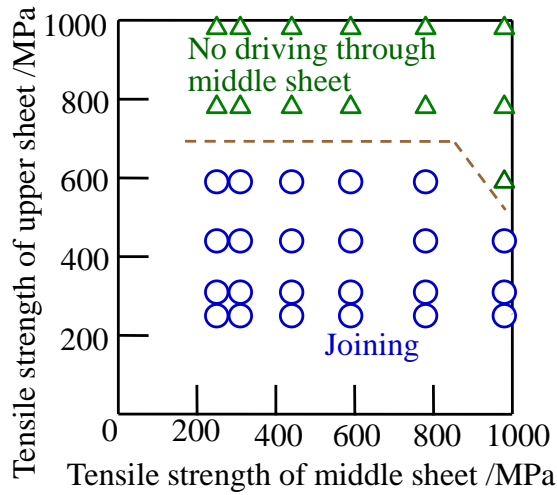


**Fig. 16.** Effects of strengths of upper and middle sheets on joinability for upper and middle steel and lower aluminium alloy sheet.

#### 4.2. Extension of joining range

The shape of the die was optimised to extend the joining range to harder sheets. As the diameter  $D$  of the die cavity and the depth  $d$  of the central die bottom increase, the load for piercing the middle sheet decreases as shown in Fig. 17, i.e. harder sheets are pierced due to the reduction in pressure acting at the tip of the rivet skirt. When the diameter of the die cavity is  $D=11$  mm and the depth of the central die bottom is  $d=1.5$  mm, the load is smaller than the yielding load of the whole rivet and these dimensions were employed for the following riveting operation.

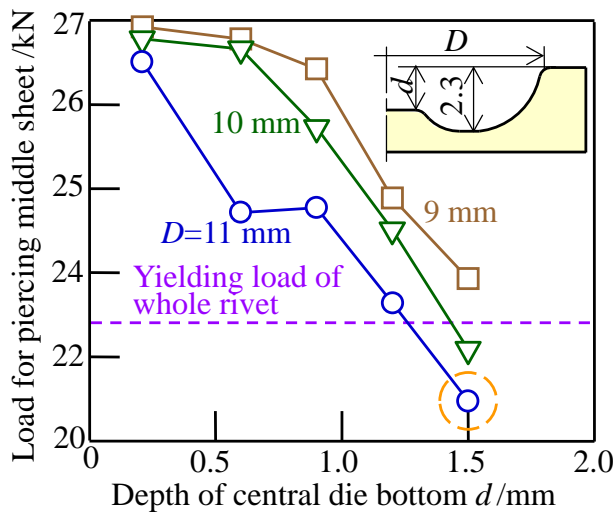


**Fig. 17.** Relationship between load for piercing middle sheet and depth of central die bottom for upper: SPFC980, middle: SPCC and lower: A5052-H34.

The upper SPFC980, middle SPCC and lower A5052-H34 sheets are joined with the optimised die as shown in Fig. 18, whereas the joining did not succeed for the conventional die as shown in Fig. 14 (b). Since the riveting load decreases for the optimised die, the dull tip was prevented and piercing became easy.

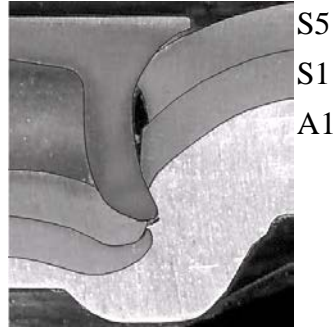


**Fig. 18.** Cross-sectional shape for upper: SPFC980 (S5), middle: SPCC (S1) and lower: A5052-H34 (A1) joined with optimised die.

The joining range for the high strength steel sheets was considerably improved in Fig. 19 from that shown in Fig. 16. The high strength steel and aluminium alloy sheets were successfully joined except for upper and middle SPFC980.

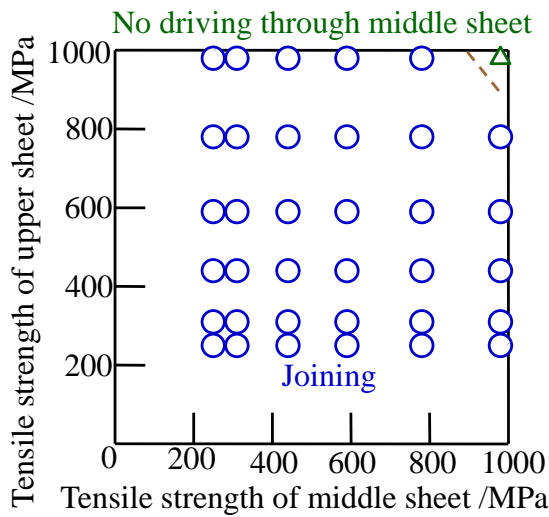


**Fig. 19.** Improvement of joinability of three sheets using optimised die.

The relationship between the maximum load measured from the cross-tension test and the tensile strength is given in Fig. 20. For the steel sheets having a tensile strength above 400 MPa, not only the extension of the joining range but also the increase in joint strength is obtained by optimisation of die shape.

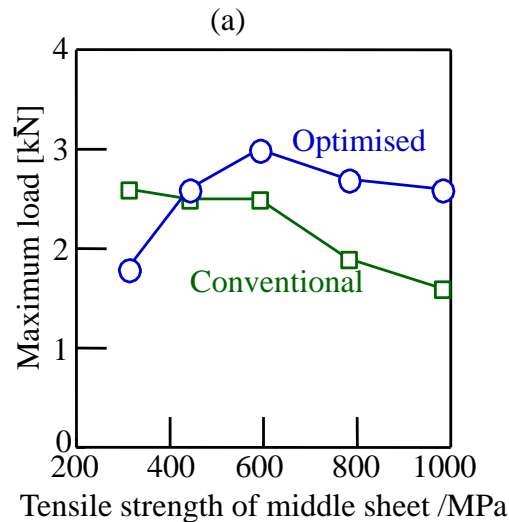
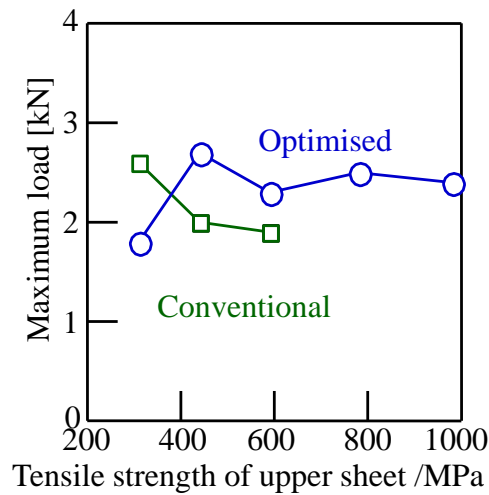


**Fig. 20.** Relationship between maximum load and tensile strength in cross-tension test for (a) middle: SPCC and (b) upper: SPCC.

## 5. Conclusions

Since self-pierce riveting is a cold joining process by plastic deformation, dissimilar sheets having different melting temperatures can be joined. For the dissimilar sheets, it is significantly desirable to join high strength steel and aluminium alloy sheets effective for lightweight automobiles. In addition, the self-pierce riveting process has the advantage of joining multiple sheets, because the sheets except for the lower sheet are merely pieced with the rivet. In self-pierce riveting of multiple dissimilar sheets, plastic deformation of sheets and rivet is controlled to generate a sufficient interlock. However, it is not easy to pierce the rivet into the hard high strength steel sheets, because the strength of the sheets approaches that of the rivet. Since not only high strength but also proper ductility is required for the rivet, the increase in rivet strength is limited. The optimisation of shapes of a die and rivet using finite element simulation is the most effective approach for improving the joinability of self-pierce riveting.

## References

- Abe, Y., Kato, T., Mori, K., 2006. Joinability of aluminium alloy and mild steel sheets by self piercing rivet. *Journal of Materials Processing Technology* 177 (1-3), 417–421.
- Abe, Y., Kato, T., Mori, K., 2009. Self-piercing riveting of high tensile strength steel and aluminium alloy sheets using conventional rivet and die. *Journal of Materials Processing Technology* 209 (8), 3914–3922.
- Abe, Y., Mori, K., Kato, T., 2012. Joining of high strength steel and aluminium alloy sheets by mechanical clinching with dies for control of metal flow. *Journal of Materials Processing Technology* 212 (4), 884–889.
- Abe, Y., Mori, K., Norita, K., 2013. Gradually contacting punch for improving stretch flangeability of ultra-high strength steel sheets. *CIRP Annals - Manufacturing Technology* 62 (1), 263–266.
- Barnes, T.A., Pashby, I.R., 2000. Joining techniques for aluminium spaceframes used in automobiles: Part II - adhesive bonding and mechanical fasteners, *Journal of Materials Processing Technology* 99 (1-3), 72–79.
- Coelho, R.S., Kostka, A., dos Santos, J.F., Kaysser-Pyzalla, A., 2012. Friction-stir dissimilar welding of aluminium alloy to high strength steels: mechanical properties and their relation to microstructure. *Materials Science and Engineering: A* 556,175–183.
- He, X., Pearson, I., Young, K., 2008. Self-pierce riveting for sheet materials: State of the art. *Journal of Materials Processing Technology* 199 (1–3), 27–36.
- Kato, T., Abe, Y., Mori, K., 2007. Finite element simulation of self-piercing riveting of three aluminium alloy sheets. *Key Engineering Materials* 341, 1461–1466.
- Lai, M., Brun, R., 2007. Latest developments in sheet metal forming technology and materials for automotive application: the use of ultra high strength steels at Fiat to reach weight reduction at sustainable costs. *Key Engineering Materials* 344, 1–8.
- Ma, N., Murakawa, H., 2010. Numerical and experimental study on nugget formation in resistance spot welding for three pieces of high strength steel sheets, *Journal of Materials Processing Technology* 210 (14), 2045–2052.
- Mori, K., Kato, T., Abe, Y., Ravshanbek, Y., 2006. Plastic joining of ultra high strength steel and aluminium alloy sheets by self piercing rivet, *CIRP Annals - Manufacturing Technology* 55 (1), 283–286.
- Mori, K., Akita, K., Abe, Y., 2007. Springback behaviour in bending of ultra-high-strength steel sheets using CNC servo press. *International Journal of Machine Tools & Manufacture* 47 (2), 321–325.
- Mori, K., Abe, Y., Suzui, Y., 2010. Improvement of stretch flangeability of ultra-high strength steel sheet by smoothing of sheared edge. *Journal of Material Processing Technology* 210 (4), 653–659.
- Mori, K., Abe, Y., Kato, T., 2012. Mechanism of superiority of fatigue strength for aluminium alloy sheets joined mechanical clinching and self-pierce riveting. *Journal of Materials Processing Technology* 212 (9), 1900–1905.
- Mori, K., Bay, N., Fratini, L., Micari, F., Tekkaya, A.E., 2013. Joining by plastic deformation. *CIRP Annals - Manufacturing Technology* 62 (2), 673–694.
- Neugebauer, R., Bouzakis, K.D., Denkena, B., Klocke, F., Sterzing, A., Tekkaya, A.E., Wertheim, R., 2011. Velocity effects in metal forming and machining processes. *CIRP Annals - Manufacturing Technology* 60 (2), 627–650.
- Sartkulvanich, P., Kroenauer, B., Golle, R., Konieczny, A., Altan, T., 2010. Finite element analysis of the effect of blanked edge quality upon stretch flanging of AHSS. *CIRP Annals - Manufacturing Technology* 59 (1), 279–282.



## Figure captions

- Fig. 1.** Self-pierce riveting process of multiple sheets. (a) Driving through upper sheet, (b) driving through sheets except for upper sheets and (c) joining by formation of interlock.
- Fig. 2.** Self-pierce riveting of multiple aluminium alloy A5052-H34 sheets having thicknesses of (a) 0.5-0.5-0.5-2 mm, (b) 0.5-1-2 mm, (c) 1-0.5-2 mm and (d) 1.5-2 mm.
- Fig. 3.** Tools used for experiment of self-pierce riveting.
- Fig. 4.** Deforming behaviour of rivet and sheets obtained from finite element simulation of self-pierce riveting of upper and lower: A5052-H34 (A1) and middle: SPCC (S1) for  $t_u=0.5$  mm,  $t_m=1.2$  mm and  $t_l=1.5$  mm. (a)  $s=0.0$  mm, (b)  $s=1.0$  mm, (c)  $s=3.8$  mm and (d)  $s=5.0$  mm.
- Fig. 5.** Cross-sectional shapes of rivet and sheets obtained from experiment of riveting of upper and lower: A5052-H34 (A1) and middle: SPCC (S1) for  $t_u=0.5$  mm,  $t_m=1.2$  mm and  $t_l=1.5$  mm.
- Fig. 6.** Defects for self-pierce riveting. (a) No driving through middle sheet, upper: SPCC (S1), middle and lower: A5052-H34 (A1),  $t_u=t_m=0.8$  mm,  $t_l=1.5$  mm and (b) rupture of lower sheet, upper and middle: A5052-H34 (A1), lower: SPCC (S1),  $t_u=0.5$  mm,  $t_m=t_l=1.0$  mm.
- Fig. 7.** Joinability for three sheets obtained from experiment. (a) Upper and middle: aluminium, lower: steel, (b) upper and middle: steel, lower: aluminium, (c) upper: aluminium, middle and lower: steel, (d) upper and lower: steel, middle: aluminium, (e) upper: steel, middle and lower: aluminium and (f) Upper and lower: aluminium, middle: steel.
- Fig. 8.** Comparison between cross-sectional shapes obtained from experiment for  $t_u=t_m=1.0$  mm,  $t_l=1.5$  mm. (a) Upper and lower: A5052-H34 (A1), middle: SPCC (S1) and (b) Upper: SPCC (S1), middle and lower: A5052-H34 (A1).
- Fig. 9.** Comparison between riveting loads from finite element simulation for  $t_u=t_m=1.0$  mm,  $t_l=1.5$  mm.
- Fig. 10.** Deforming behaviour of rivet and sheets obtained from finite element simulation for  $t_u=t_m=1.0$  mm,  $t_l=1.5$  mm. (a) Upper and lower: A5052-H34 (A1), middle: SPCC (S1) and (b) upper: SPCC (S1), middle and lower: A5052-H34 (A1).
- Fig. 11.** Cross-tension test for measuring strength of joints.
- Fig. 12.** Fractures in cross-tension test for upper and lower: A5052-H34 and middle: SPCC. (a) Fracture of upper sheet,  $t_u=0.5$  mm,  $t_m=1.2$  mm,  $t_l=1.5$  mm and (b) fracture of lower sheet,  $t_u=0.8$  mm,  $t_m=1.2$  mm,  $t_l=1.0$  mm.
- Fig. 13.** Relationship between maximum load and interlock area in cross-tension test for one mild steel and two aluminium alloy sheets.
- Fig. 14.** Comparison between cross-sectional shapes for (a) upper: SPCC (S1), middle: SPFC980 (S5) and (b) upper: SPFC980 (S5), middle: SPCC (S1).
- Fig. 15.** Deforming behaviour of rivet and sheets obtained from finite element simulation of self-pierce riveting of high strength steel, mild steel and aluminium alloy sheets for  $t_u=t_m=1$  mm,  $t_l=2.5$  mm. (a) Upper: SPCC (S1), middle: SPFC980 (S5) and (b) upper: SPFC980 (S5), middle: SPCC (S1).
- Fig. 16.** Effects of strengths of upper and middle sheets on joinability for upper and middle steel and lower aluminium alloy sheet.
- Fig. 17.** Relationship between load for piercing middle sheet and depth of central die bottom for upper: SPFC980, middle: SPCC and lower: A5052-H34.
- Fig. 18.** Cross-sectional shape for upper: SPFC980 (S5), middle: SPCC (S1) and lower: A5052-H34 (A1) joined with optimised die.
- Fig. 19.** Improvement of joinability of three sheets using optimised die.
- Fig. 20.** Relationship between maximum load and tensile strength in cross-tension test for (a) middle: SPCC and (b) upper: SPCC.

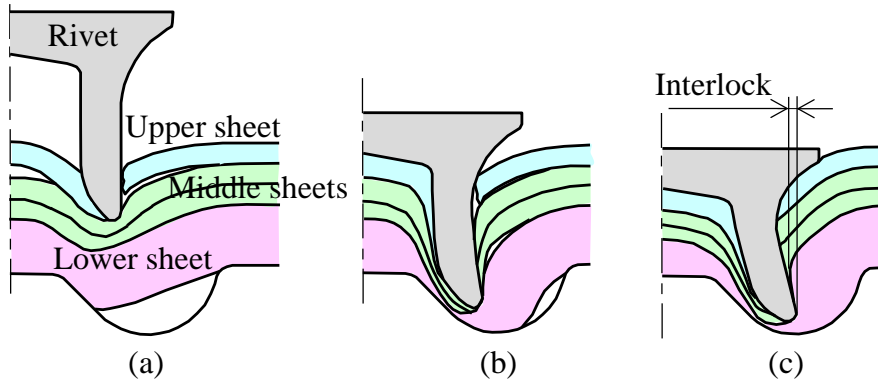


**Fig. 1.** Self-pierce riveting process of multiple sheets. (a) Driving through upper sheet, (b) driving through sheets except for upper sheets and (c) joining by formation of interlock.

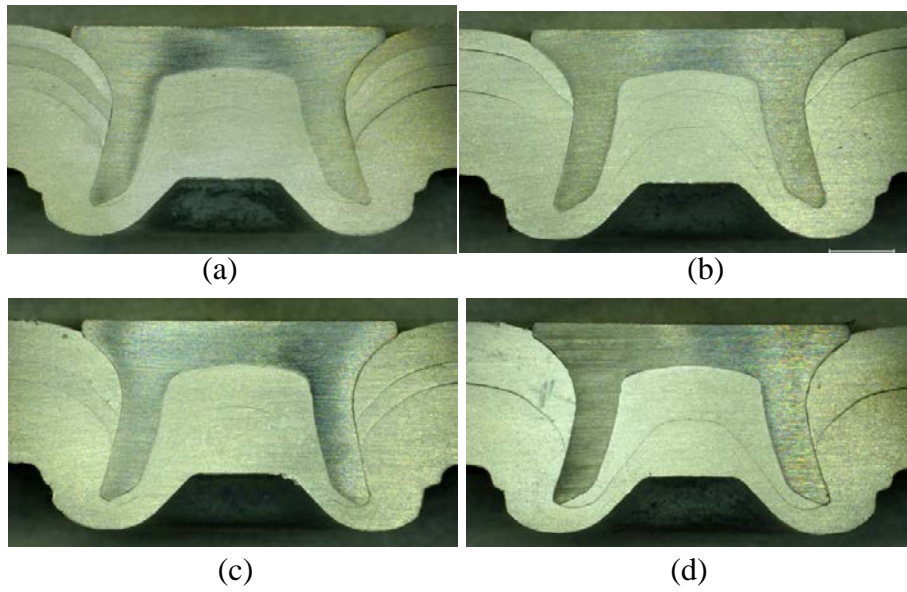


**Fig. 2.** Self-pierce riveting of multiple aluminium alloy A5052-H34 sheets having thicknesses of (a) 0.5-0.5-0.5-2 mm, (b) 0.5-1-2 mm, (c) 1-0.5-2 mm and (d) 1.5-2 mm.

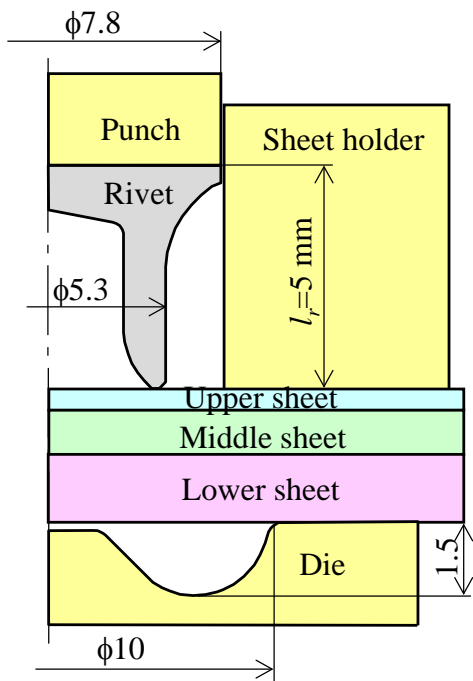


**Fig. 3.** Tools used for experiment of self-pierce riveting.

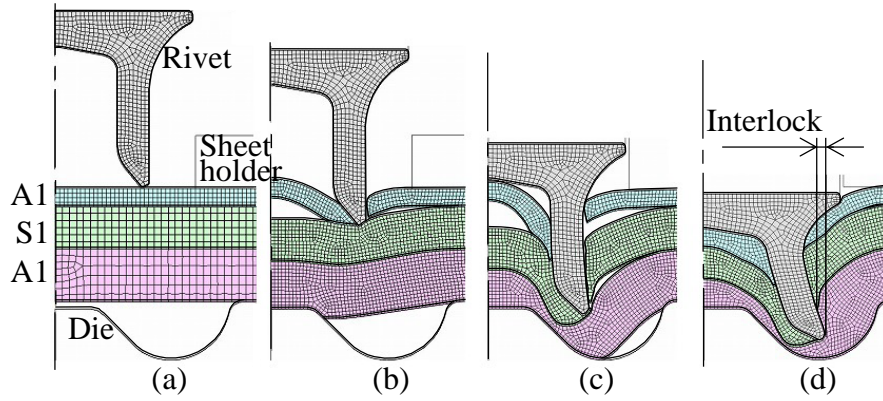


**Fig. 4.** Deforming behaviour of rivet and sheets obtained from finite element simulation of self-pierce riveting of upper and lower: A5052-H34 (A1) and middle: SPCC (S1) for  $t_u=0.5$  mm,  $t_m=1.2$  mm and  $t_l=1.5$  mm. (a)  $s=0.0$  mm, (b)  $s=1.0$  mm, (c)  $s=3.8$  mm and (d)  $s=5.0$  mm.

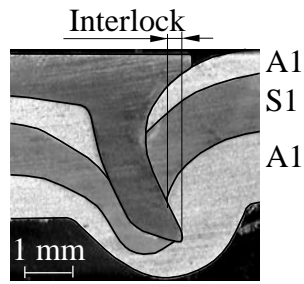


**Fig. 5.** Cross-sectional shapes of rivet and sheets obtained from experiment of riveting of upper and lower: A5052-H34 (A1) and middle: SPCC (S1) for  $t_u=0.5$  mm,  $t_m=1.2$  mm and  $t_l=1.5$  mm.

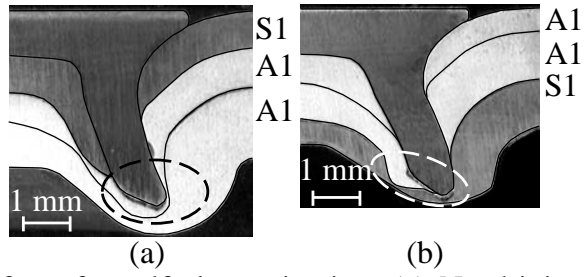


**Fig. 6.** Defects for self-pierce riveting. (a) No driving through middle sheet, upper: SPCC (S1), middle and lower: A5052-H34 (A1),  $t_u=t_m=0.8$  mm,  $t_l=1.5$  mm and (b) rupture of lower sheet, upper and middle: A5052-H34 (A1), lower: SPCC (S1),  $t_u=0.5$  mm,  $t_m=t_l=1.0$  mm.



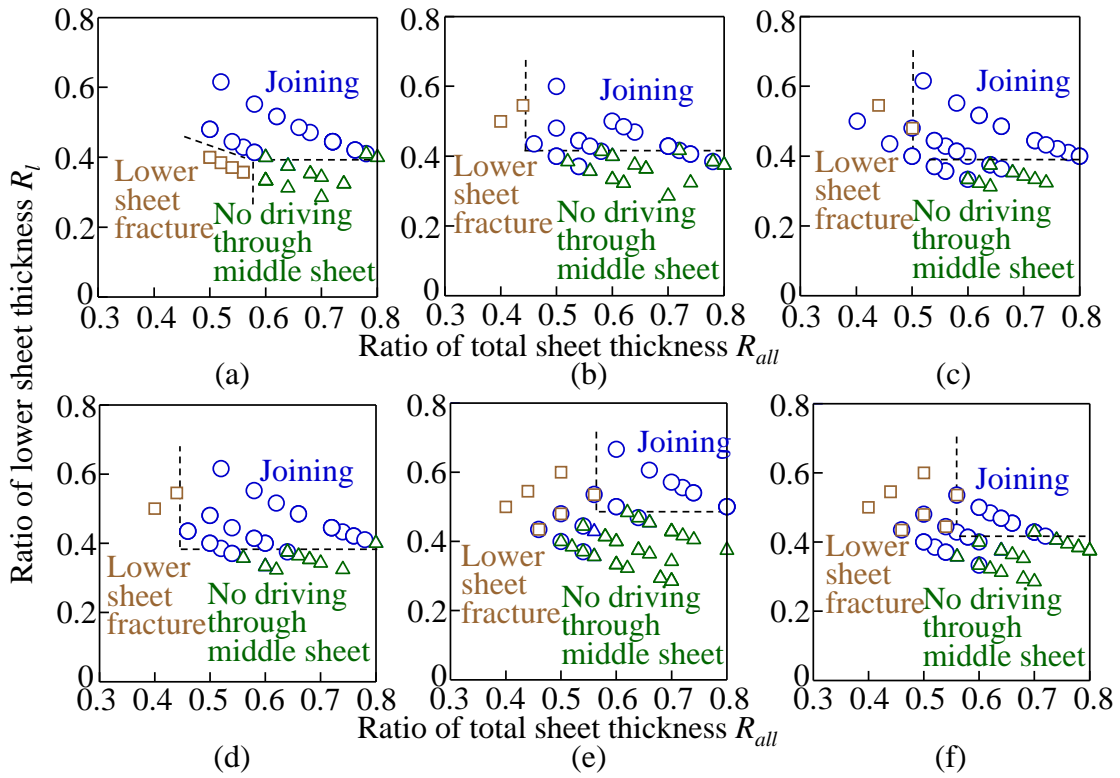


**Fig. 7.** Joinability for three sheets obtained from experiment. (a) Upper and middle: aluminium, lower: steel, (b) upper and middle: steel, lower: aluminium, (c) upper: aluminium, middle and lower: steel, (d) upper and lower: steel, middle: aluminium, (e) upper: steel, middle and lower: aluminium and (f) Upper and lower: aluminium, middle: steel.

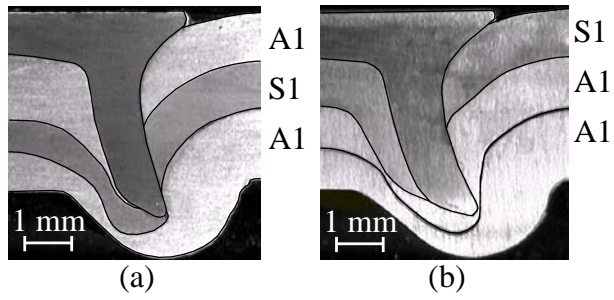


**Fig. 8.** Comparison between cross-sectional shapes obtained from experiment for  $t_u = t_m = 1.0$  mm,  $t_l = 1.5$  mm. (a) Upper and lower: A5052-H34 (A1), middle: SPCC (S1) and (b) Upper: SPCC (S1), middle and lower: A5052-H34 (A1).

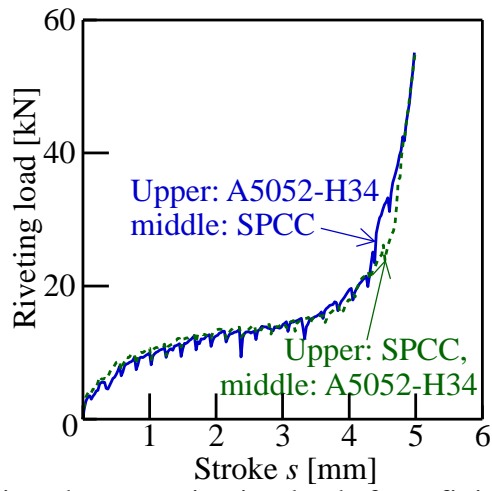


**Fig. 9.** Comparison between riveting loads from finite element simulation for  $t_u = t_m = 1.0$  mm,  $t_l = 1.5$  mm.

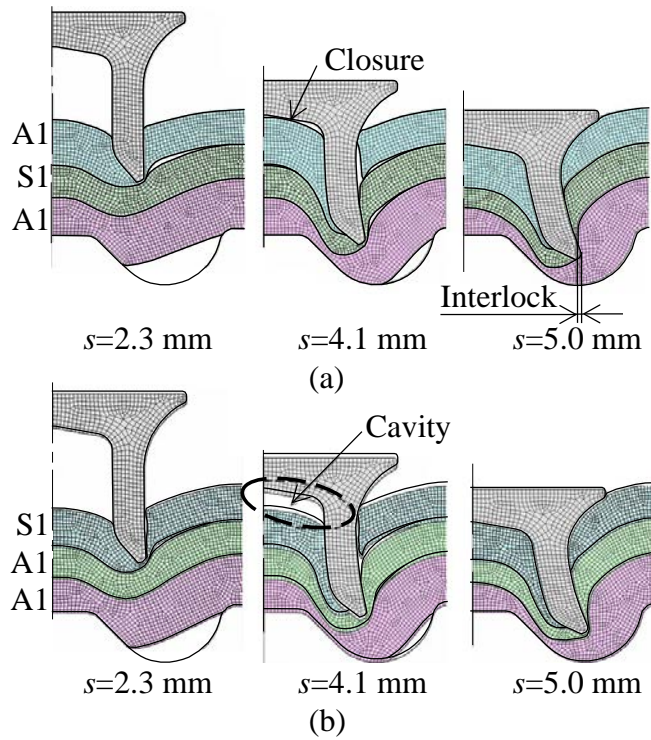


**Fig. 10.** Deforming behaviour of rivet and sheets obtained from finite element simulation for  $t_u = t_m = 1.0$  mm,  $t_l = 1.5$  mm. (a) Upper and lower: A5052-H34 (A1), middle: SPCC (S1) and (b) upper: SPCC (S1), middle and lower: A5052-H34 (A1).

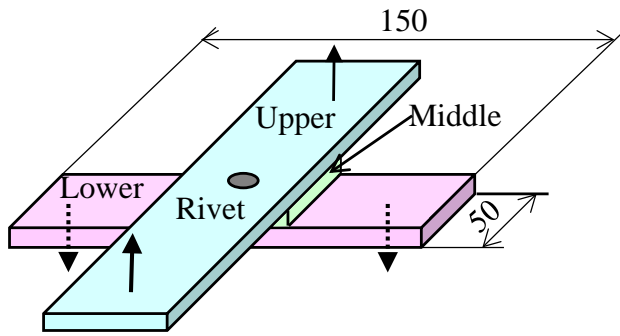


**Fig. 11.** Cross-tension test for measuring strength of joints.

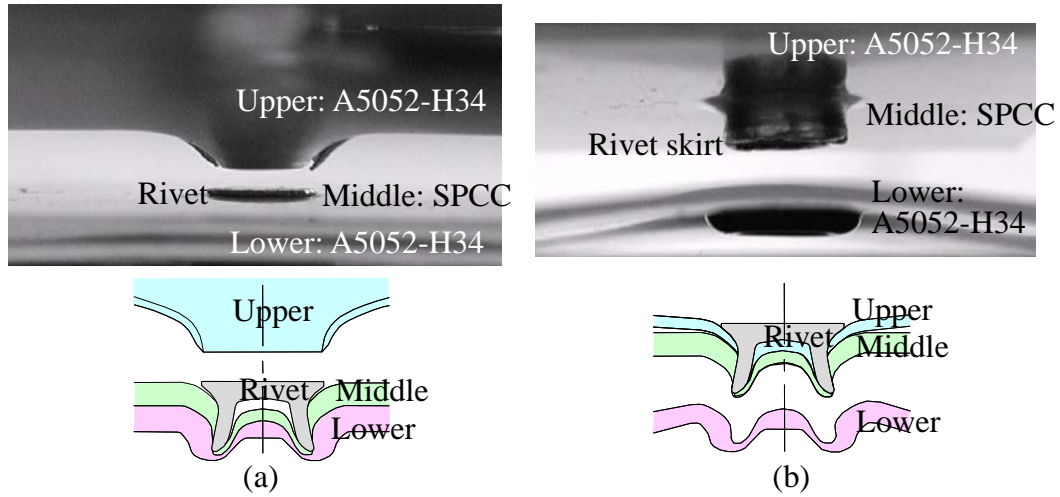


**Fig. 12.** Fractures in cross-tension test for upper and lower: A5052-H34 and middle: SPCC. (a) Fracture of upper sheet,  $t_u=0.5$  mm,  $t_m=1.2$  mm,  $t_l=1.5$  mm and (b) fracture of lower sheet,  $t_u=0.8$  mm,  $t_m=1.2$  mm,  $t_l=1.0$  mm.

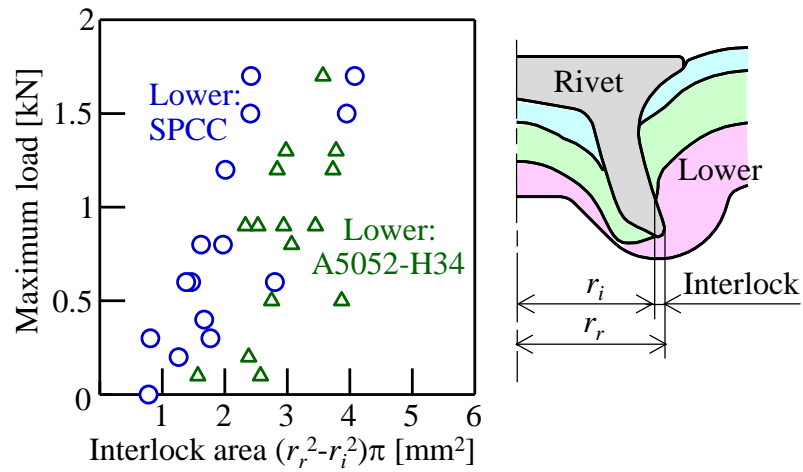


**Fig. 13.** Relationship between maximum load and interlock area in cross-tension test for one mild steel and two aluminium alloy sheets.



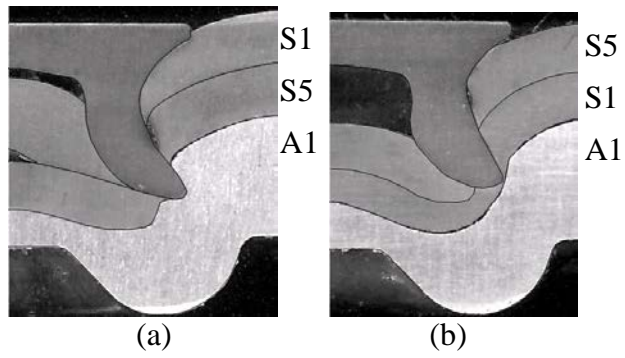


**Fig. 14.** Comparison between cross-sectional shapes for (a) upper: SPCC (S1), middle: SPFC980 (S5) and (b) upper: SPFC980 (S5), middle: SPCC (S1).

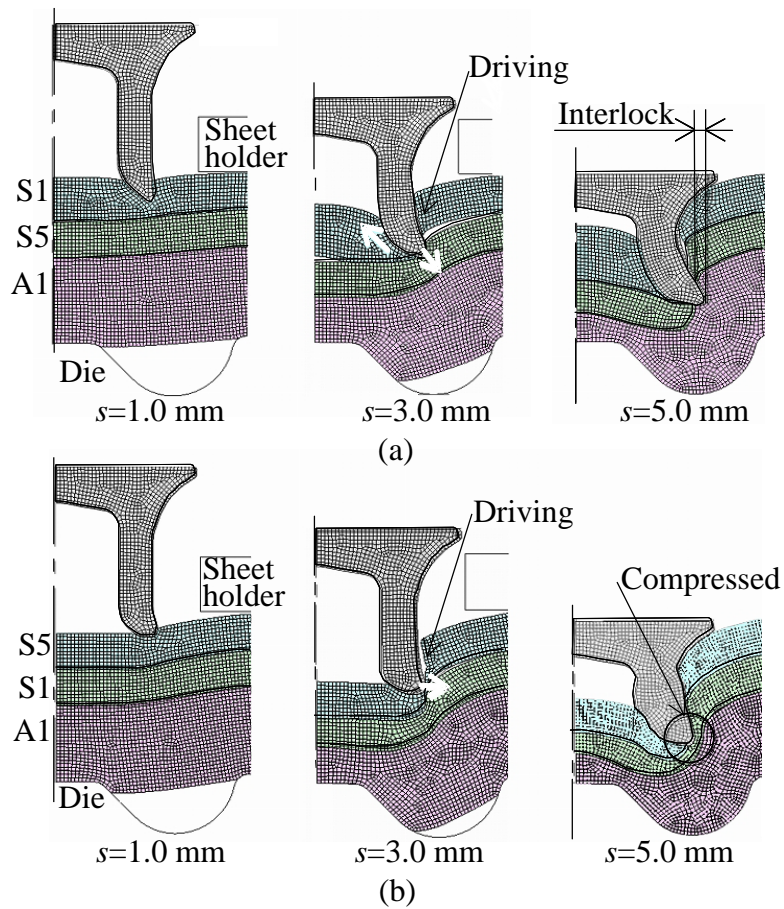


**Fig 15.** Deforming behaviour of rivet and sheets obtained from finite element simulation of self-pierce riveting of high strength steel, mild steel and aluminium alloy sheets for  $t_u = t_m = 1$  mm,  $t_l = 2.5$  mm. (a) Upper: SPCC (S1), middle: SPFC980 (S5) and (b) upper: SPFC980 (S5), middle: SPCC (S1).

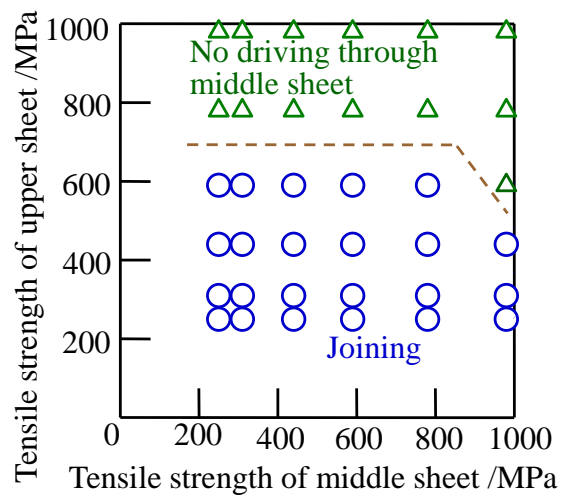


**Fig. 16.** Effects of strengths of upper and middle sheets on joinability for upper and middle steel and lower aluminium alloy sheet.

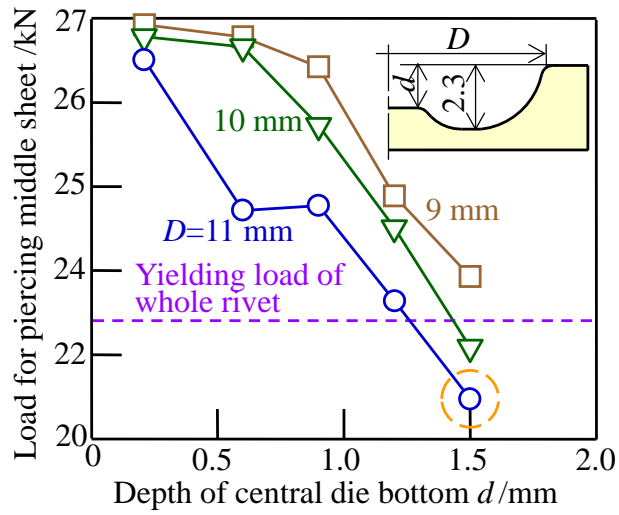


**Fig. 17.** Relationship between load for piercing middle sheet and depth of central die bottom for upper: SPFC980, middle: SPCC and lower: A5052-H34.

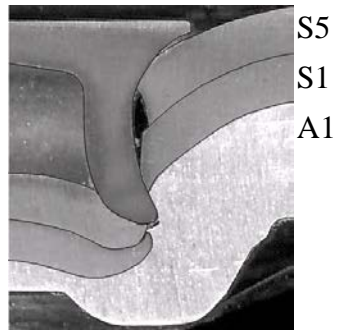


**Fig. 18.** Cross-sectional shape for upper: SPFC980 (S5), middle: SPCC (S1) and lower: A5052-H34 (A1) joined with optimised die.

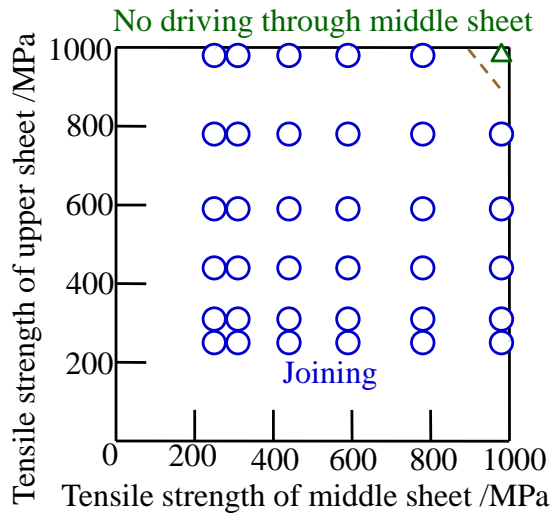
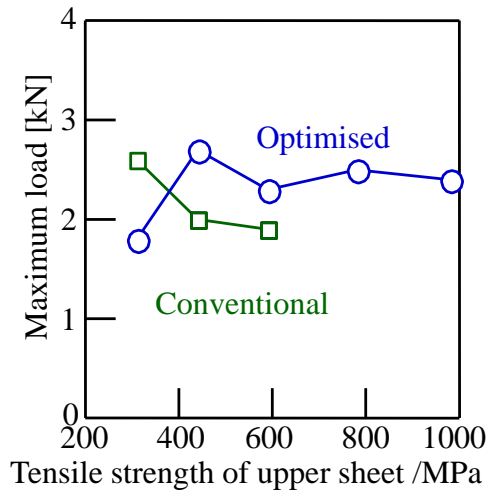
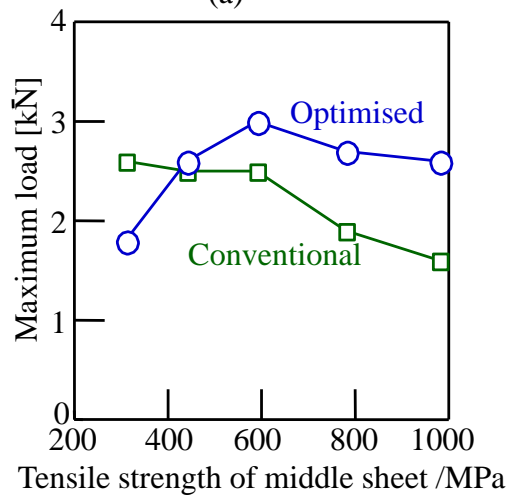


**Fig. 19.** Improvement of joinability of three sheets using optimised die.



(a)



(b)

**Fig. 20.** Relationship between maximum load and tensile strength in cross-tension test for (a) middle: SPCC and (b) upper: SPCC.

**Table 1**

Mechanical properties of sheets and rivet used for self-pierce riveting.

Sheet	Material	Thickness [mm]	Elongation [%]	Yield stress [MPa]	Tensile strength [MPa]	Flow stress curve [MPa]
SPCC (S1)	Mild steel	1.0	33	203	334	$\sigma = 530\varepsilon^{0.25}$
SPFC440 (S2)	Dual-phase steel	1.0	25	343	473	$\sigma = 774\varepsilon^{0.18}$
SPFC590 (S3)		1.0	18	424	623	$\sigma = 979\varepsilon^{0.16}$
SPFC780 (S4)		1.0	20	503	764	$\sigma = 1187\varepsilon^{0.15}$
SPFC980 (S5)		1.0	17	838	976	$\sigma = 1337\varepsilon^{0.08}$
		2.0	18	862	1057	$\sigma = 1531\varepsilon^{0.13}$
A5052-H34 (A1)	Aluminium-magnesium alloy	1.0	8.2	205	258	$\sigma = 387\varepsilon^{0.12}$
		2.5	9.3	196	244	$\sigma = 353\varepsilon^{0.11}$
Rivet	0.35%-carbon boron steel			1850		$\sigma = 1955\varepsilon^{0.014}$